



**HAL**  
open science

## Overhanging shapes of freezing sessile drops under continuous liquid supply

Rémy Herbaut, Philippe Brunet, Laurent Royon, Laurent Limat

► **To cite this version:**

Rémy Herbaut, Philippe Brunet, Laurent Royon, Laurent Limat. Overhanging shapes of freezing sessile drops under continuous liquid supply. *International Journal of Thermal Sciences*, 2019, 140, pp.135-143. 10.1016/j.ijthermalsci.2019.02.043 . hal-02343315

**HAL Id: hal-02343315**

**<https://hal.science/hal-02343315>**

Submitted on 2 Nov 2019

**HAL** is a multi-disciplinary open access archive for the deposit and dissemination of scientific research documents, whether they are published or not. The documents may come from teaching and research institutions in France or abroad, or from public or private research centers.

L'archive ouverte pluridisciplinaire **HAL**, est destinée au dépôt et à la diffusion de documents scientifiques de niveau recherche, publiés ou non, émanant des établissements d'enseignement et de recherche français ou étrangers, des laboratoires publics ou privés.

## Overhanging shapes of freezing sessile drops under continuous liquid supply

R. Herbaut,<sup>1, a)</sup> P. Brunet,<sup>1</sup> L. Royon,<sup>2</sup> and L. Limat<sup>1</sup>

<sup>1)</sup>*Laboratoire MSC, UMR 7057 CNRS, Université Paris Diderot, Paris, France*

<sup>2)</sup>*Laboratoire LIED, UMR 8236 CNRS, Université Paris Diderot, Paris, France*

(Dated: 6 December 2018)

To predict the shape of solidifying material onto a substrate is currently motivating an increasing number of studies related to additive manufacturing. Here we consider the solidification of a liquid drop on a cold substrate, below the freezing temperature, under continuous feeding at a constant flow-rate through a thin needle placed above. We compare experimental shapes to those predicted by a theoretical model where heat transfer is mainly due to conduction within the solid and when the inner flow is neglected. Hence, this is an analogous of Stefan problem for a sessile drop, with additional feeding of liquid. We show that, depending on the control parameters, namely the initial angle, substrate temperature and flow-rate, different shapes are observed, in particular original overhanging ones. We provide a simple model, which is in very good agreement with experiments. We then discuss on the limitations of the model.

PACS numbers: Valid PACS appear here

Keywords: Solidification, Droplet, Phase Change

---

<sup>a)</sup>Laboratoire MSC, UMR 7057 CNRS, Université Paris Diderot, Paris, France; Electronic mail: [remy.herbaut@univ-paris-diderot.fr](mailto:remy.herbaut@univ-paris-diderot.fr)

## I. INTRODUCTION

The shape of liquid free-surface solidifying from a cold substrate has motivated numerous studies related to heat exchange, crystal growth<sup>1</sup>, geophysics<sup>2,3</sup>, prevention of frost formation<sup>4,5</sup> or additive manufacturing<sup>6</sup>. For the latter application, it is often required to deposit on a solid a given amount of fluid with well controlled three-dimensional shape<sup>6</sup>. However, the shape results from a complex interplay between spreading dynamics with fast advancing contact-line during early stages, and heat transfer, phase change, mass conservation and shaping by surface tension and gravity during late stages<sup>7</sup>. In applied situations, an additional complexity comes from the non-newtonian rheology of the material used, e.g. a melted polymer that cools down and solidifies at ambient temperature.

Here, we consider a model situation of a liquid drop gently deposited on a substrate colder than the freezing temperature, that progressively freezes and is simultaneously inflated from above, by a continuous supply of liquid at ambient temperature and fixed flow-rate. As the liquid meets the substrate, it first spreads radially under the antagonist effects of inertia, viscosity and surface tension<sup>8</sup> and reaches a final radius of arrest that depends on the substrate temperature<sup>9</sup>. As liquid is constantly poured on top of the freezing basal melt, it eventually freezes and forms a solid puddle that grows both upwards and radially outwards. Figure 1 shows a typical sequence of the freezing of such a continuously fed drop.

This situation is reminiscent of a sessile drop freezing on a cold substrate, that forms pointy shapes in the final stage of freezing<sup>10-13</sup>. The formation of this pointy shape was explained from a simple static model with mass conservation coupled to the geometry of the drop. It was found that it originates from that liquid water is denser than ice<sup>10-12</sup> and that the tip angle only depends on the density ratio between solid and liquid phases<sup>12,13</sup>. Therefore, this singular shape is not observed for most substances, which are denser in their solid phase. Another example of a material denser in its liquid phase is silicium, and the formation of a forest of similar pikes was observed during cycles of melting and solidification<sup>14</sup>, showing a general character in these pointy shapes.

Related to the present study, the shape of freezing wax puddles formed by the successive impact of droplet sprays onto a cold substrate was investigated by Schiaffino and Sonin<sup>15,16</sup>. Their study was focused on the arrest and spreading criterion of the puddle at the contact-line, and found a pinning criterion based on a threshold value for the contact angle between

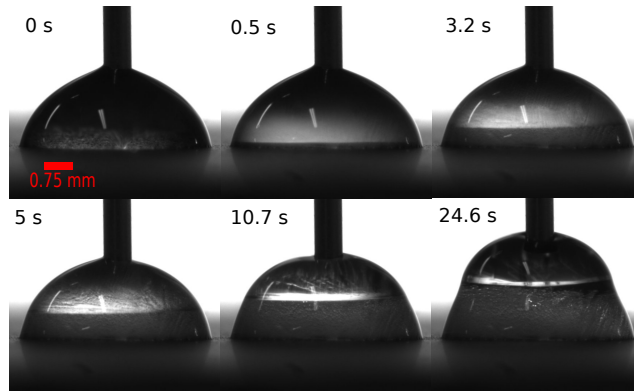


FIG. 1. Successive shapes of a drop of water freezing from its base on a cold substrate, under continuous feeding. After a first stage of fast spreading, the liquid is laterally pinned and reaches its final basal diameter. Then, the drop thickens and grows upwards as the freezing front progresses also upwards.

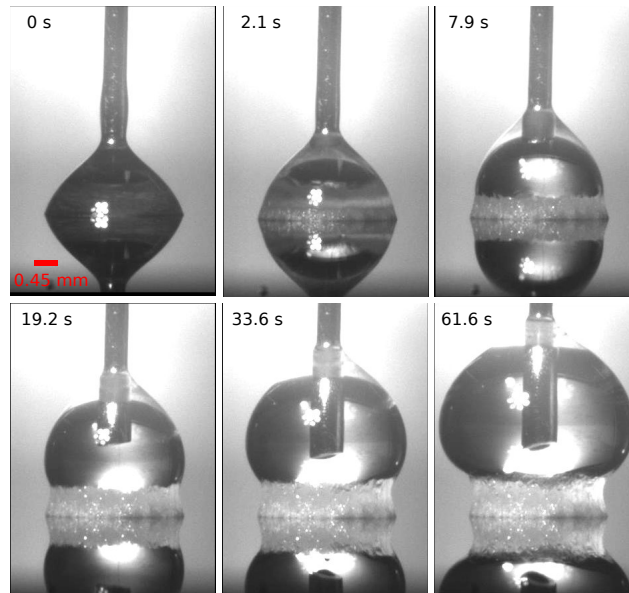


FIG. 2. Successive shapes of a drop of hexadecane freezing from its base on a cold substrate, under continuous feeding. Flow-rate  $Q = 0.1 \mu\text{l/s}$ ,  $\Delta T = 4^\circ$ . Under these conditions, the freezing drop adopts an overhanging shape, which constitutes its final one before the liquid on top collapses and falls under gravity.

the liquid and the basal solid. Another study revisited the pinning criterion in terms of critical frozen volume near the triple line<sup>17</sup>. More recently, a kinetic criterion based on the advancing velocity of a spreading drop was quantitatively and successfully tested<sup>9</sup>. The apparent discrepancies between these studies reveal that the pinning seems dependent on the geometry and history of spreading.

Besides the computation of the final shape, various studies investigated the time evolution of the freezing front (i.e. the Stefan problem adapted to convex and time-evolving geometry), which departs from the trivial square-root law expected for a half-space geometry<sup>18–20</sup>. Other recent studies added the effect of supercooling<sup>21</sup>, of thermal convection<sup>22</sup>, and of using ice as the substrate<sup>23</sup>, revealing more complex behavior. Overall, the peculiar shape of the drop itself has a significant influence on the heat transfer between the substrate, the solidified material and the remaining liquid on top. Our study is also motivated by fundamental questions on this non-trivial coupling between the drop shape and thermal gradients within the solid and the liquid.

How does a continuous supply of liquid influence the final shape of the frozen ice deposit ? We address this question both experimentally and numerically. The theoretical model, inspired from Snoeijer and Brunet<sup>12</sup>, is quasi-static : it assumes a straight horizontal front, it neglects the flow dynamics in the liquid and the resulting convection. Though, by comparing both experimental and numerical shapes, we find very good quantitative agreement for a large investigated range of control parameters. In particular, we observed and explained overhanging shapes for the drop and we determine the maximal aspect ratio such a drop can get before the liquid flows over by gravity before freezing. In this prospect, this study is also of interest for the understanding of the first steps of the formation of natural structures by successive deposition of ice, like in stalagmites<sup>24–26</sup> or snow penitents<sup>27</sup>. However, under specific conditions, we noticed a strong discrepancy between experiments and theory, which is seemingly related to the appearance of the phenomenon of recalescence. From a liquid drop initially in undercooling situation, recalescence appears as a brief (typically  $t \ll 1$  s) formation of a mixed ice-and-liquid state within the whole drop, before the solid-liquid front rises<sup>17,21</sup>.

The paper is organised as follow : we first describe the experimental setup in Section II, then we present theoretical elements of the problem in Section III. In Section IV, we compare experimental and numerical shapes for various sets of control parameters. In Section

V, we give possible explanation for the few cases where discrepancy is observed between experiments and numerics. Finally, Section VI concludes the paper.

## II. EXPERIMENTAL SETUP

The experimental setup is depicted in Fig 3. A thin (350 microns thick) silicon wafer is cooled at controlled temperature with a Peltier cell (RadioSpare : CP1.4-127-06L-RTV) installed below, in contact with a heat dissipator and powered by a stabilised power supply. Thermal contact between the silicon wafer and the Peltier cell is ensured with thermal paste. The wafer temperature is controlled with a thermocouple in contact to the silicon wafer.

A vertical needle of diameter  $d=0.7$  mm, placed a distance between 1 to 5 mm from above the surface, pours the liquid at constant flow-rate, which eventually forms the growing drop. The flow rate  $Q$  is controlled by a syringe pump (HARVARD APPARATUS B-67085) and ranges between  $10^{-11}$  to  $10^{-8}$   $m^3s^{-1}$ , or 0.01  $\mu\text{l/s}$  to 10  $\mu\text{l/s}$ . Two different liquids have been used : water and hexadecane, which liquid density  $\rho_l$ , solid density  $\rho_s$ , viscosity  $\eta$  and surface tension at  $T = T_m$ ,  $\gamma$ , are respectively :  $\rho_l = 1000$  and  $774$   $\text{kg.m}^{-3}$  in liquid phase,  $\rho_s = 917$  and  $833$   $\text{kg.m}^{-3}$  in solid phase,  $\eta = 1.793 \cdot 10^{-3}$  and  $0.003$  Pa.s and  $\gamma = 0.07564$  and  $0.028$  N/m. Their melting temperature  $T_m$  are respectively 273 K and 291.5 K at atmospheric pressure. The thermal conductivity  $k$  of the solid, latent heat  $L$  and heat capacity  $C_{pl}$  of the liquid are respectively 2.1 W/m/K and 0.15 W/m/K,  $3.34 \times 10^5$  J/kg and  $2.3 \times 10^5$  J/kg, 4185 J/kg/K and 2310 J/kg/K.

In order to prescribe different wetting conditions, the substrate can be chemically treated with a grafting of a self-assembled monolayer (SAM) of a fluorosilane : 1H,1H,2H,2H per-fluorodecyltrichlorosilane, hereafter denoted as PFTS, ensuring non-wetting conditions for water and partial wetting conditions for hexadecane. This grafting with covalent bonds is known to ensure a robust and durable coating, both mechanically and chemically. When any sign of coating degradation was detected, we replaced the wafer with a new coating.

The time evolution of the shape is recorded with a side-view camera (Imaging Source DMK 23U445), as in the sequence of Figure 1.

We identified three main control parameters that significantly influence the final shape of the frozen drop: the substrate temperature  $T_p$  (through its difference with  $T_m$ , namely  $\Delta T = T_m - T_p$ ), the flow-rate  $Q$  and the initial contact-angle  $\theta_0$ . The injection temperature

$T_i$  was found to play no significant influence on the final frozen shape for both liquids, so we opted to operate at ambient temperature (20°C) for convenience.

A typical experiment begins after the drop has spread to its final basal radius  $R_0$ , with the solidification starting from the bottom in contact with the cold substrate. A solidification front rising upwards is observed. The typical final height  $h$  of frozen drops is smaller than roughly 5 mm. This maximal height is ruled by the limit situation occurring when the thermal gradient  $\nabla_z T = \frac{T_m - T_p}{h}$  becomes too weak to ensure the cooling and freezing of the freshly poured liquid. Once the limit height is attained, the liquid that accumulated on top is at some point going to flow down the solid by gravity. Before this limit height is reached, the solidification front velocity decreases inside the droplet, following Stefan's law<sup>1,28</sup>. The remaining liquid on top of the solid, has a typical volume  $V$ , with  $V^{1/3} < l_c$  (where the capillary length  $l_c = \left(\frac{\gamma}{\rho g}\right)^{1/2}$ ), so that its shape is ruled mainly by surface tension and adopts that of a spherical cap. In the case of a relatively low flow-rate  $Q$ , the experiment finishes when the solid front reaches the needle location. In the case of a relatively high  $Q$ , the experiment ends when some liquid falls down the formed solid, breaking the axisymmetry and preventing the further rise of the front. The typical timescale of experiments is between 10 and 30 s.

### III. THEORETICAL MODEL

We present a theoretical model that predicts the shape of the ice drop, inspired from Snoeijer and Brunet<sup>12</sup>. The front is assumed to be horizontal, see Fig. 3, while the remaining liquid sits on the solid puddle with an angle  $\theta(z)$ . We also assume that the heat flux dominates mainly through the solid, and that the heat from the surrounding vapour is negligible. The shape of the ice drop is entirely defined by  $R(z)$ , as the shape remains axisymmetric. Overall, this model includes no dynamics nor convection, only mass conservation. In this sense, the ratio between liquid and solid density  $\nu = \frac{\rho_s}{\rho_l}$  has proven to be a crucial quantity for the shape of the ice drop, in particular for the appearance of a final pointy shape<sup>12,13</sup>, which is observed only for liquids expanding upon freezing ( $\nu < 1$ ) like water.

Following the assumptions of figure 3, the model contains three geometrical quantities: the liquid volume  $V(z)$ , the radius of the ice/liquid interface  $R(z)$  and the contact angle of

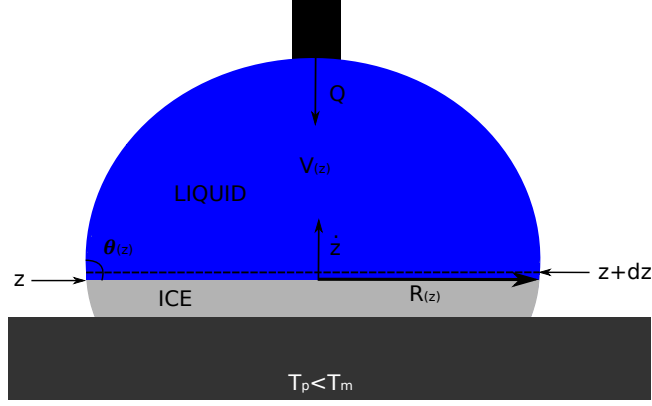


FIG. 3. Geometrical model for the solidification of droplet with continuous feeding rate  $Q$ . The liquid/solid interface is assumed to be flat, horizontal and the unfrozen liquid is assumed to adopt the shape of a spherical cap. Consequently, the axisymmetric shape is entirely defined by  $R(z)$ , and the liquid drop forms an angle  $\theta(z) = \tan^{-1}(-\frac{dz}{dR})$  with the ice front.

liquid with ice  $\theta(z)$ . The assumption of a flat front was questioned in previous studies<sup>13</sup>, and it turns out that a curved front intersecting the free-surface with a right angle was more realistic to predict the final shape of pointy ice drops. In the present study though, a flat horizontal front could fairly reproduce the experimental shapes. With millimeter-sized drops, gravity can be neglected and the liquid that sits on the solid base, adopts the shape of a spherical cap. Hence, the volume is given by:

$$\frac{V_{sc}}{R^3} = \frac{\pi}{3} \left( \frac{2 - 3 \cos \theta + \cos^3 \theta}{\sin^3 \theta} \right) \quad (1)$$

From simple trigonometry, we relate  $R(z)$  and  $\theta(z)$  as:

$$\frac{dz}{dR} = -\tan \theta \quad (2)$$

We now write the local relationship coming from the balance between the solidifying liquid and the liquid brought by the injector  $Qdt$ . In the layer of thickness  $dz$  above the solid front, the volume of freezing liquid is  $-\nu\pi R^2 dz$ . Taking  $dV(z)$  as the infinitesimal variation of liquid volume when the front rises from  $z$  to  $z + dz$ , mass conservation yields:

$$\frac{dV}{dz} = -\nu\pi R^2 + \frac{Q}{\dot{z}} \quad (3)$$

with  $\dot{z}$  stands for the speed of the solidification front. This speed can be estimated by the classical relationship deduced from the Stefan problem, assuming a constant and vertical temperature gradient  $\nabla_z T = \frac{T_m - T_p}{z} = \frac{\Delta T}{z}$  and considering that the temperature is continuous at the solidification front, and equal to the melting temperature  $T_m$ :

$$\dot{z} = \frac{k\Delta T}{\rho_s L z} \quad (4)$$

with  $k$  the thermal conductivity of the solid phase and  $L$  the latent heat. This Stefan condition is deduced from energy conservation : indeed the amount of heat generated by the phase change is balanced by the difference in heat flux from either side of the solid-liquid front. The assumption of a linear temperature profile across the ice layer is justified, considering that ice or solid hexadecane have a significantly larger conductivity (2.1 and 0.15 W/m/K) than that of ambient air (0.024 W/m/K). Now considering the liquid volume as a function of  $R$  and  $z$ , we can write the differential equation of  $V_{sc}$  as:

$$\frac{dV_{sc}}{dz} = -\frac{1}{\tan \theta} \frac{\partial V_{sc}}{\partial R} + \frac{\partial V_{sc}}{\partial \theta} \frac{\partial \theta}{\partial z} \quad (5)$$

With a bit of algebra, i.e. working out the partial derivatives with trigonometry relationships<sup>12</sup>, equations (2), (3) and (5) can be simplified into a system of two coupled differential equations for  $R$  and  $\theta$  as:

$$\frac{d\theta}{dz} = -\frac{1}{R} \left[ \left( \nu - \frac{Q}{2\pi R^2 \dot{z}} \right) - \left( 1 - \nu + \frac{Q}{2\pi R^2 \dot{z}} \right) (2 \cos \theta + \cos^2 \theta) \right] \quad (6)$$

$$\frac{dR}{dz} = -\frac{1}{\tan \theta} \quad (7)$$

Once the initial radius  $R_0 = R(z = 0)$  and angle  $\theta$  are fixed, the system of equations (6) and (7) fully determines the shape of the solid drop  $R(z)$ .

We solve this system of equations, numerically using *Matlab*. The computed shapes are compared with experiments taking the same set of parameters. In particular, we compared shapes obtained with the two liquids (water and hexadecane), having different physical properties, and in particular different values for the density ratio  $\nu$ , respectively equal to 0.917 and 1.076. Hereafter, we show examples of experimental and computed shapes under different sets of parameters ( $Q$ ,  $\Delta T$  and  $\theta_0$ ).

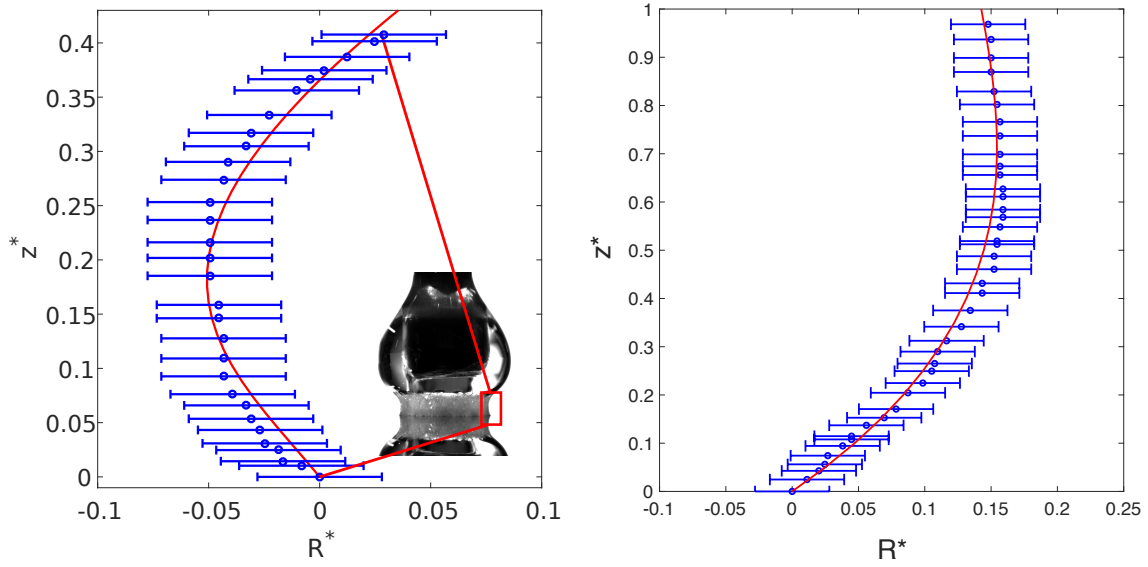


FIG. 4. Experimental and numerical shapes of a frozen drop. (a) Hexadecane with initial contact angle  $\theta_0 = 40^\circ$  and initial radius  $R_0 = 1.71$  mm.  $\Delta T = 4$  °C and  $Q=0.83$   $\mu\text{l/s}$  (b) Water with initial contact angle  $\theta_0 = 120^\circ$  and initial radius  $R_0 = 2$  mm.  $\Delta T = 9$  °C and  $Q=0.32$   $\mu\text{l/s}$

#### IV. COMPARISON BETWEEN EXPERIMENTAL AND COMPUTED SHAPES

Figures 4-(a) and (b) show typical examples of superimposed experimental and numerical shapes, i.e. the dimensionless height  $z^* = \frac{z}{R_0}$  versus dimensionless radius  $R^* = \frac{R-R_0}{R_0}$ , with very good agreement between both. Error bars are due to the uncertainty in the determination of the shape position, as the roughness of the solid-air interface diffuses the light from the back. Figure 4-(a) corresponds to an initial condition with partial wetting ( $\theta_0 \leq \frac{\pi}{2}$ ), obtained with hexadecane on PFTS, and figure 4-(b) corresponds to a non-wetting initial condition ( $\theta_0 \geq \frac{\pi}{2}$ ) with water on PFTS, with other control parameters being specified in the caption. It is remarkable that in both situations,  $\frac{dR}{dz}$  changes sign above a critical  $z$ . The situation of a drop freezing without additional liquid supply<sup>12</sup>, exhibits this change of sign for  $\theta_0 \geq \frac{\pi}{2}$ , but not for  $\theta_0 \leq \frac{\pi}{2}$ . Hence, the resulting overhanging shape shown in Fig. 4-(a) can be attributed to the continuous supply of liquid.

To check more quantitatively the influence of flow-rate  $Q$ , a series of experiments were carried out over a broad range of values of  $Q$ , while keeping  $\Delta T$  and  $\theta_0$  constant. Results are shown in Figure 5 for three values of  $Q$ , which again evidences a good agreement between

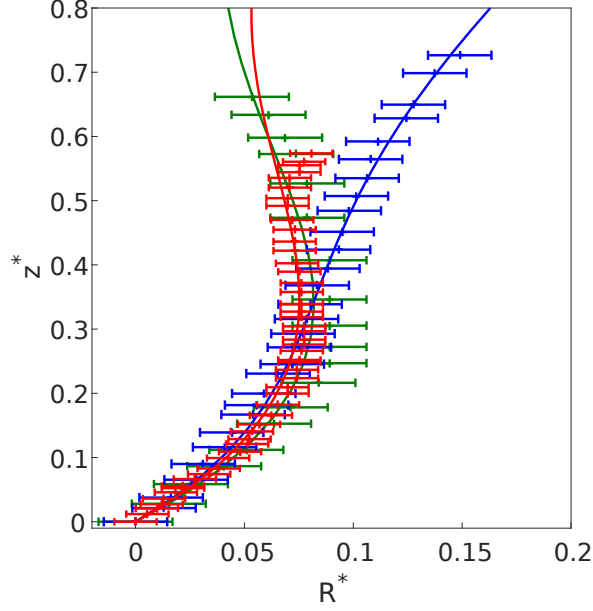


FIG. 5. Experimental and numerical shapes of frozen ice (water) drops for different flow-rate  $Q$ , with  $\Delta T=9$  °C and  $\theta =120^\circ$ . The data points (experiments) and related plain lines (numerics) correspond to :  $Q=0.16$   $\mu\text{l/s}$  (green)  $Q=0.32$   $\mu\text{l/s}$  (red) and  $Q=0.5$   $\mu\text{l/s}$  (blue)

the model and experimental results. These shapes also show that increasing flow-rate leads to a broader, thicker shape for the frozen drop, which can sometimes be overhanging, for large enough  $Q$  (here, the blue curve for  $Q=0.5$   $\mu\text{l/s}$ ).

By a systematic comparison between experiments and numerics, we validate the model over a large range of experimental parameters. Hence, we confidently addressed the calculation of the frozen shape and its systematic dependence on the different control parameters mentioned above :  $Q$ ,  $\Delta T$  and  $\theta_0$ . The complexity of the shape makes it difficult to find a relevant quantity to characterise it. We opted for two choices :

- the radius of the frozen shape at  $z = 2$  mm. The choice was motivated by (a) that frozen ice shape reaches this height for most parameters sets (i.e. before the supplied liquid from the top falls down), and (b) that the influence of control parameters can be more sensitive at relatively high  $z$  than in the first stages of the freezing. Furthermore, this value is close to the capillary length of water (equal to  $l_c = 2.76$  mm at 273 K).

- the radius of the frozen shape at the highest inflection point  $z_i$  of the curve  $R(z_i)$ , i.e. where  $\left(\frac{d^2R}{dz^2}\right)_{z=z_i} = 0$  and the value of  $z_i$  itself. This inflection point corresponds to the steepest overhanging slope. This is also the moment when the radius slows down its increase

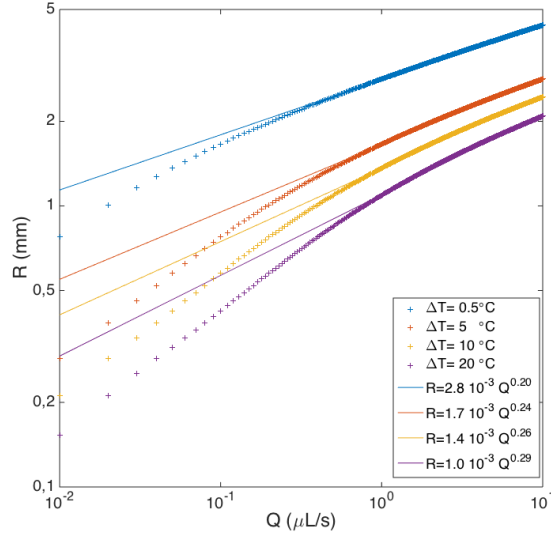


FIG. 6. Calculated radius of the frozen drop (distilled water) at a height of 2 mm versus flow rate for different values of  $\Delta T$ . Other parameters are :  $\theta_0 = \pi/2$ ,  $R_0=1$  mm.

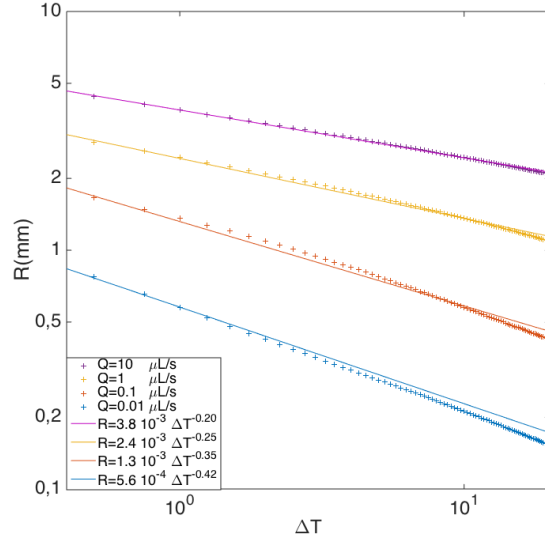


FIG. 7. Calculated radius of the frozen drop (distilled water) at a height of 2 mm versus undercooling  $\Delta T$ , for different flow-rates  $Q$ . Other parameters are :  $\theta_0 = \pi/2$ ,  $R_0=1$  mm.

with  $z$ .

Figures 6, 7 and 8 are plots of  $R$  ( $z=2$  mm) obtained from the numerical results of the model. In Fig. 6, we addressed the influence of flow-rate on the radius, and as stated above it turns out that thicker shapes are obtained for increasing  $Q$ , and the typical radius follows

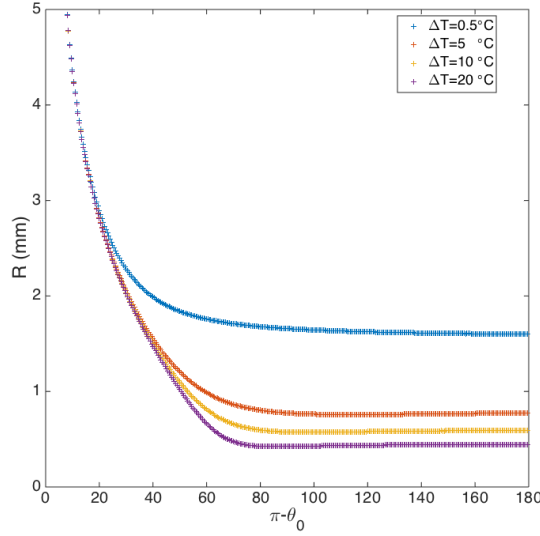


FIG. 8. Calculated radius of the frozen drop (distilled water) at a height of 2 mm versus  $(\pi - \theta_0)$  and different values of  $\Delta T$ . Other parameters are :  $Q = 0.1 \mu\text{l/s}$ ,  $R_0 = 1 \text{ mm}$ .

a power law  $R \sim Q^\alpha$ , with the coefficient  $\alpha$  ranging between 0.20 and 0.29. It is also remarkable that the value of  $\alpha$  is only slightly dependent on the undercooling  $\Delta T$ .

Figure 7 presents the influence of  $\Delta T$  on the typical radius. A stronger undercooling leads to thinner shapes, which can be understood as that when  $\Delta T$  increases, the supplied liquid freezes more quickly and it is less susceptible to spread radially and inflate the shape. Of course, this effect is more acute at smaller  $Q$ . The following power laws comes out from the results :  $R \sim (\Delta T)^{-\beta}$ , with  $\beta$  ranges from 0.20 to 0.42 depending on the flow-rate. Under the extreme situation of a very small  $Q$  ( $= 0.01 \mu\text{l/s}$ ) and high  $\Delta T$  ( $30^\circ\text{C}$ ), the radius can be smaller than  $200 \mu\text{m}$ .

Figure 8 shows the dependence of the radius versus the angle  $(\pi - \theta_0)$ , for different values of  $\Delta T$ . Under partial wetting conditions ( $\pi - \theta_0 \geq 90^\circ$ ), the initial angle has almost no influence on  $R$ . Conversely, for non-wetting conditions ( $\theta_0 \geq 90^\circ$ ), the shape gets thicker for increasing  $\theta_0$ . The higher the undercooling  $\Delta T$ , the sharper the increase of  $R$  with  $\theta_0$ .

Now we consider the radius of the frozen drop at  $z = z_i$ . Although being significant to determine the location of the shape inflection, this height does not keep a fixed value over the described ranges of parameters. First, let us determine the height  $z_i$  versus  $Q$  and  $\Delta T$ . These values are plotted in figures 9 and 10.

Figure 9 shows the evolution of  $z_i$  with  $Q$ , for different  $\Delta T$ . For very small  $\Delta T$ ,  $z_i$

monotonically decreases with  $Q$  following a power law  $z_i \sim Q^{\alpha'}$ . The value of  $\alpha'$  roughly equals  $-\frac{2}{9}$ . For higher  $\Delta T$ ,  $z_i$  first increases with  $Q$  then decreases for larger values of  $Q$ , following a similar power law as the one for small  $\Delta T$ , with an exponent of  $-\frac{2}{9}$ . It is striking that whatever the value of  $\Delta T$ ,  $z_i$  keeps smaller than 2.6 mm, which is roughly the capillary length  $l_c$  for water.

Figure 10 presents the dependence of  $z_i$  on  $\Delta T$ . For low enough flow-rates ( $Q \ll 1 \mu\text{l/s}$ ), the typical height of the inflection point increases monotonically with  $\Delta T$ , with an increase becoming slighter at high  $Q$ . For higher  $Q$  ( $\geq 1 \mu\text{l/s}$ ), the trend is different :  $z_i$  first increases with  $\Delta T$  then decreases at higher  $\Delta T$  (plot at  $Q = 1 \mu\text{l/s}$ ), or even decreases monotonically (plot at  $Q = 10 \mu\text{l/s}$ ).

Obviously, the dependence of  $z_i$  on the different experimental parameters, has significant influence on the radius at  $z_i$ ,  $R(z_i)$ , giving trends which can be different from those related to the radius at fixed height. Figure 11 shows  $R(z_i)$  versus  $Q$  for different  $\Delta T$ . Overall, one notices a significant increase of the drop radius, which is sharper for lower  $Q$ , and that converges to a plateau value (slightly lower than 2 mm) at higher  $Q$ .

In Figure 12, the evolution of  $R(z_i)$  with  $\Delta T$  is plotted. For high  $Q$ , the radius is almost independent on  $\Delta T$  and roughly equal to 2 mm, while it significantly decreases with  $\Delta T$  at smaller  $Q$ . Again, the competition between the freezing rate and the rate of liquid supply is clearly illustrated here. While under a stronger undercooling, the liquid freezes before accumulating on top, and hence the shape tends to be slender, the increase of  $Q$  makes this shape being thicker and almost independent on  $\Delta T$ .

## V. DISCUSSION AND LIMITATIONS OF THE MODEL

The originality of the frozen shapes resulting from freezing under continuous liquid supply, is their ability to take overhanging shapes. The reason appears in eq. (3) : in the absence of liquid feeding ( $Q=0$ ), mass conservation would simply lead to  $\frac{dV}{dz} < 0$ , which corresponds to  $R(z)$  decreasing with  $z$ . Conversely, in our situation the sign of  $\frac{dV}{dz}$  depends on the value of  $\frac{\nu\pi R^2 \dot{z}}{Q} = \frac{\nu\pi R^2 k \Delta T}{Q \rho_s L z}$  : if the ratio is  $\leq 1$ ,  $\frac{dV}{dz} \geq 0$  and conversely if the ratio is  $\geq 1$ ,  $\frac{dV}{dz} \leq 0$ . During freezing, the thickness of the frozen layer  $z$  increases from 0 up to a few mm, while other quantities keep constant. Hence,  $\frac{dV}{dz}$  should be negative during the first stages of solidification (as  $z$  is very small) and become positive at large enough  $z$ , according to what

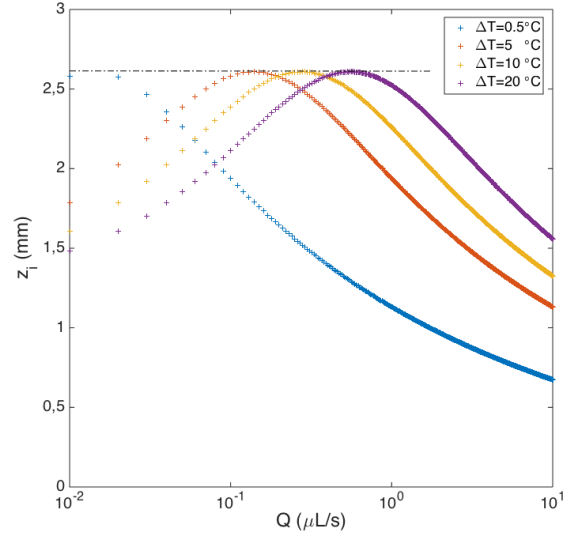


FIG. 9. Calculated height of the highest inflection point  $z_i$ , versus flow rate for the case of water and different values of  $\Delta T$ . Other parameters are :  $\theta_0 = \pi/2$ ,  $R_0=1$  mm.

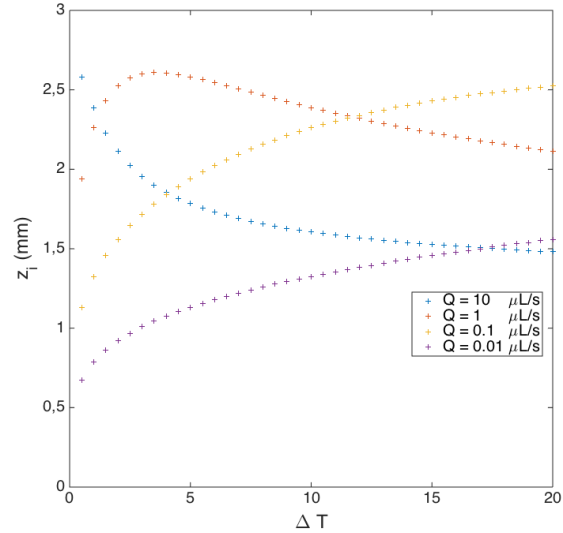


FIG. 10. Calculated height of the highest inflection point  $z_i$ , versus undercooling  $\Delta T$ , for distilled water. Other parameters are :  $\theta_0 = \pi/2$ ,  $R_0=1$  mm.

has been stated just before. Hence, there is an increase of the volume of liquid accumulating on top and it leads to an increase of  $R(z)$  with  $z$ . To some extent, the increase of  $R(z)$  should counterbalance the decrease of the thermal gradient  $\Delta T/z$  as the freezing goes on. This explains why overhanging shapes are observed. This is well captured by the model,

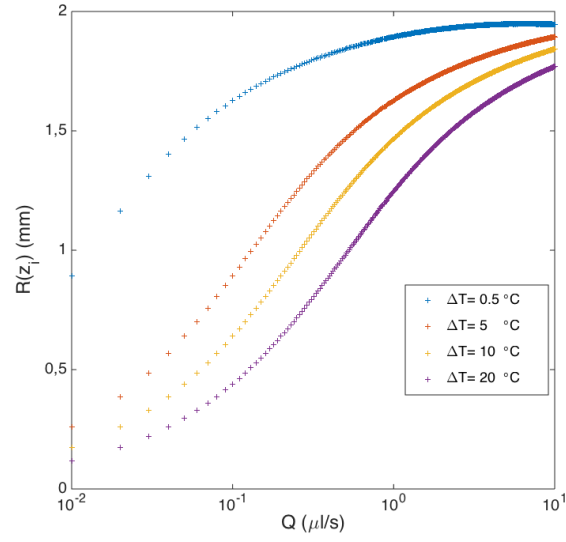


FIG. 11. Calculated radius of the frozen drop (distilled water) at  $z_i$ , versus flow rate, for different values of  $\Delta T$ . Other parameters are :  $\theta_0 = \pi/2$ ,  $R_0=1$  mm.

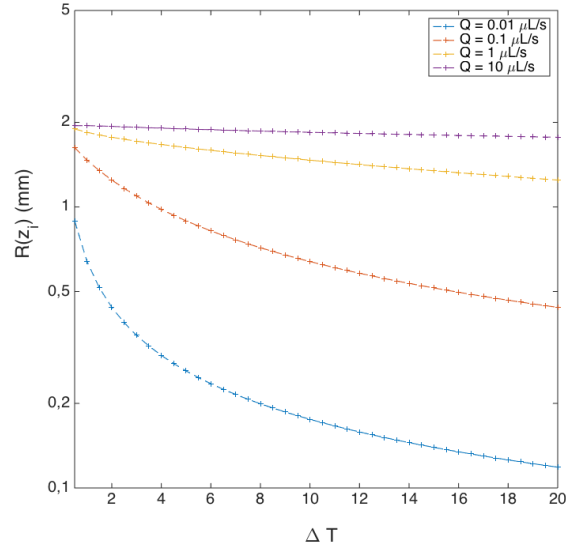


FIG. 12. Calculated radius of the frozen drop (distilled water) at  $z_i$ , versus undercooling  $\Delta T$ . Other parameters are :  $\theta_0 = \pi/2$ ,  $R_0=1$  mm.

according to the trends shown in the previous section.

However, the validity of the model is limited and two main situations have been found to show discrepancies between the predicted and measured shapes :

- a) when the supplied liquid does not stay on top of the already frozen shape and simply

flows down the foot of ice before it freezes. This is due to the limited power of the cooling element, compared to the rate of liquid supply. Drops with very pronounced overhanging shapes often constitute the first signs of this regime, which is out of the scope of the present study.

b) with water only, sometimes recalescence occurs prior to the appearance of the ice-water front, as observed in previous studies<sup>17,21</sup>. By recalescence, we denote the observation of a sudden nucleation and expansion of frozen solid inside the drop which transforms the initial liquid volume into an ice-water mixture within less than one second.

Situation (a) occurs in case of either too low undercooling  $\Delta T$ , either too high flow-rate or either of shapes which become too tall (too large aspect ratio  $\frac{z}{R_0}$ ) : the model is then unable to reproduce the observed shapes. We can roughly predict when the supplied liquid will flow down before being frozen. From the rate of liquid poured from the injector during an infinitesimal duration  $\delta t$  at ambient temperature  $T_i$ , we evaluate the heat transfer required to cool it down  $T_f$  and the heat required to freeze it :

$$\delta H_i = (\rho_s L + \rho_l C_{pl} \Delta T_i) Q \delta t \quad (8)$$

where  $\Delta T_i = T_i - T_m$ . We compare this heat with the flux through the solid across the area  $\pi R^2$  :

$$\delta H_f = \frac{k \Delta T}{z} \pi R^2 \delta t \quad (9)$$

Let us first remark that in  $\delta H_i$ , the term of latent heat is generally dominant over that of thermal capacity : it requires more heat transfer to freeze a given mass of liquid than to put this liquid from ambient to freezing temperature. Quantitatively, we can evaluate a Stefan number for the heat transfer in the liquid :

$$Ste = \frac{C_{pl} \Delta T_i}{L} \quad (10)$$

which equals 0.25 for water and 0.015 for hexadecane at ambient  $T_i=20^\circ$ . Hence, for the rough estimation of  $z_{\max}$  we intend to make, we only keep the latent heat term in (8).

If we equal  $\delta H_i$  and  $\delta H_f$ , it yields :

$$\rho_s L Q \simeq \frac{k \Delta T}{z} \pi R^2$$

which allows to determine a maximal height :

$$z_{\max} = \frac{k\Delta T\pi R^2}{\rho_s LQ} \quad (11)$$

For typical values taken in experiments ( $\Delta T = 10^\circ$ ,  $Q = 0.3 \mu\text{l}$ ,  $R_0 = 2 \text{ mm}$ ) and assuming a rather constant radius ( $\theta$  keeps constant, around  $90^\circ$ ), one finds :  $z_{\max} = 2.7 \text{ mm}$  for ice/water and  $0.41 \text{ mm}$  for hexadecane. This coarse prediction is consistent with what is observed experimentally : hexadecane drops generally reach a maximal thickness of freezing between 200 microns and about one millimeter (see e.g. Fig.2), . Water drops can freeze to thicknesses up to 5 mm, also depending on  $Q$  and  $\Delta T$ . Both frozen hexadecane and ice drops eventually show the fluid accumulating on top and flowing down at some point. For this reason also, it is almost impossible to experimentally obtain shapes with radius larger than roughly 3 mm, as again gravity makes the liquid on top collapse and fall down. Let us finally remark that to neglect the contribution of the cooling of the supplied liquid should lead to slightly overestimate  $z_{\max}$ , especially for water.

Let us now focus on the latter situation (b), for which a typical sequence is depicted in Fig. 13. It shows that recalescence can appear and invade the liquid droplet during a typical time scale of less than half a second, hence much shorter than the duration required for the rise of the ice front. Indeed in the sequence, the ice front starts to appear roughly 5 s after the initial time of recalescence, and reaches the top of the drop in about 100 s. Careful observations of the drop before and after recalescence reveal that, apart that the inner liquid turns opaque, the shape remains unchanged. Therefore, the density of this amorphous ice should equal that of liquid water.

Nevertheless, the shapes computed by the model show significant discrepancy with the experimental ones. Figure 14 shows the shapes in both liquid and frozen states. Also plotted is the computed shape with the usual properties of water (plain green line) : the agreement is fine only for  $z < 0.6 \text{ mm}$ . The causes for the discrepancy remain unknown. In this case though, we found out that the profile could be correctly fitted by taking a latent heat  $L$  as a stepwise function of  $z$ . More precisely, we chose  $L$  equal to an arbitrarily small value ( $= 1 \text{ J/kg}$ ) for  $z < z_c$  and  $L$  equal to that of water freezing ( $= 334 \text{ kJ/kg}$ ) for  $z > z_c$ . The result of the numerical calculation in this case is also plotted in Fig. 14.

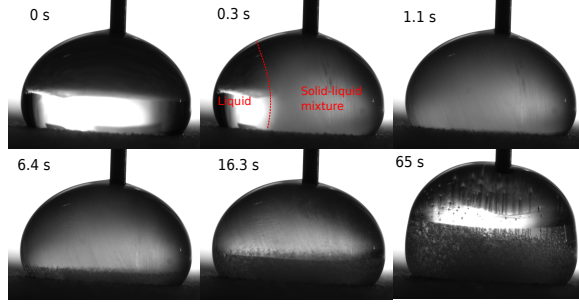


FIG. 13. Sequence of recalescence within a drop (snapshots 2 and 3), observed before the ice-water front appears at much longer times. The initial time corresponds to the first image where recalescence appears. We note that the drop shape remains unchanged during recalescence.

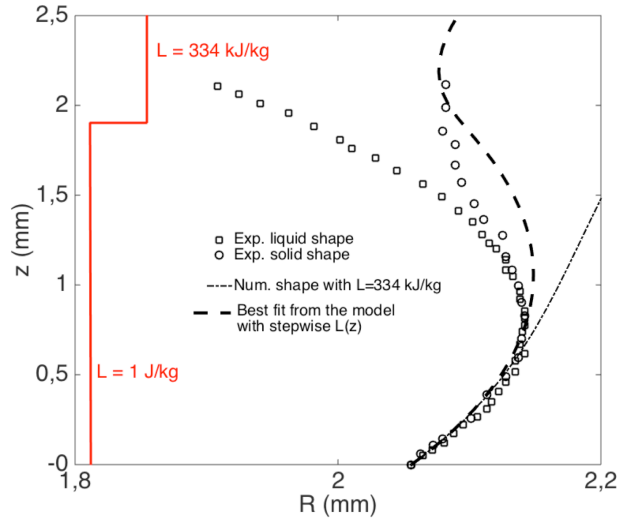


FIG. 14. Drop profile of liquid drop before (green) and after (blue) the solidification. Distilled water with initial contact angle  $\theta = 125^\circ$  and initial radius  $r = 2.15$  mm.  $Q = 1.16 \mu\text{l/s}$ .

## VI. CONCLUSIONS

The shape of a freezing sessile drop continuously fed from its top can be predicted with a quasi-static model that includes mass conservation and heat transfer via the Stefan relationship. We carried out experiments with both water and hexadecane to validate it. The predicted shapes show very good agreement with experimental ones providing two conditions are fulfilled :

- the supplied liquid remains on top of the freezing solid and does not flow over it.
- there is no recalescence in the early stages of the drop freezing. This phenomenon oc-

curing only for water, is avoided if undercooling is controlled and prevented, for instance by adding tiny amount of salts either on the substrate or in the liquid. The reason why recalescence induces discrepancy between experiments and the model remains ill-understood. At this stage, our experiments and numerical attempts suggest that the density of undercooled water seems equal to that of amorphous ice formed after recalescence, and that the experimental shapes are better fitted by taking the latent heat between water and amorphous ice at a value much smaller than the usual one between water and crystalline ice.

Under most situations, the obtained shapes show overhanging geometry, for which we quantified the dependence on the three main important parameters, namely the initial wetting angle  $\theta_0$ , the difference between freezing temperature and substrate temperature  $\Delta T$  and the feeding flow-rate  $Q$ .

Finally, besides its fundamental frame, the present study could be of interest for various applied or geophysical situations, for instance in additive manufacturing or to understand the first steps of the formation of stalagmites. We hope that this will motivate further studies with more complex - time dependent - liquid deposition and/or more powerful cooling that could enable the observation of frozen shapes with higher aspect ratio, and possibly with ripples like in some real stalagmites<sup>24-26</sup>.

## ACKNOWLEDGMENTS

We acknowledge the financial support by the Agence Nationale de la Recherche (ICEWET project : ANR-15-CE08-0031). We would like to thank E. Ablonet, J. Sébilleau and D. Legendre for fruitful discussions.

## REFERENCES

- <sup>1</sup>S. Davis, *Theory of solidification*, edited by C. U. Press (Cambridge University Press, 2001).
- <sup>2</sup>A.Baker, D.Genty, W.Dreybrodt, W.L.Barnes, N. Mockler, and J. Grapes, "Testing theoretically predicted stalagmite growth rate with Recent annually laminated samples: Implications for past stalagmite deposition," *Geochimica et Cosmochimica Acta* **62**, 393–404 (1997).

- <sup>3</sup>W. Dreybrodt and D. Romanov, “Regular stalagmites: The theory behind their shape,” *Acta Carsologica* **37**, 2–3 (2008).
- <sup>4</sup>Z. Liu, Y. Gou, J. Wang, and S. Cheng, “Frost formation on a super hydrophobic surface under convection conditions,” *J. Heat Mass Transfer* **51**, 5975–5982 (2008).
- <sup>5</sup>M. He, J. Wang, H. Li, X. Jin, J. Wang, B. Liu, and Y. Song, “Superhydrophobic film retards frost formation,” *Soft Matter* **6**, 2396–2399 (2010).
- <sup>6</sup>M. Vaezi, H. Seitz, and S. F. Yang, “A review on 3d micro-additive manufacturing technologies,” *Int. J. Adv. Manu. Technol.* **67**, 1721 (2013).
- <sup>7</sup>D. Attinger, Z. Zhao, and D. Poulikakos, “An experimental study of molten microdroplet surface deposition and solidification: Transient behavior and wetting angle dynamics,” *J. Heat Transfer* **122**, 544 (2000).
- <sup>8</sup>K. Winkels, J. Weijs, A. Eddi, and J. Snoeijer, “Initial spreading of low-viscosity drops on partially wetting surfaces,” *Phys. Rev. E* **85**, 055301(R) (2012).
- <sup>9</sup>R. de Ruiter, P. Colinet, P. Brunet, J. H. Snoeijer, and H. Gerdelblom, “Contact line arrest in solidifying spreading drops,” *Phys. Rev. Fluids* **2**, 043602 (2017).
- <sup>10</sup>A. Sanz, J. Meseguer, and L. Mayo, “The influence of gravity on the solidification of a drop,” *J. Cryst. Growth* **82**, 91–88 (1987).
- <sup>11</sup>D. Anderson, M. G. Worster, and S. H. Davis, “The case for a dynamics contact angle in containerless solidification,” *J. Cryst. Growth* **163**, 329–338 (1996).
- <sup>12</sup>J. H. Snoeijer and P. Brunet, “Pointy ice-drop: How water freezes into a singular shape,” *Semiconductors* **66**, 1238 (2001).
- <sup>13</sup>A. G. Marin, O. R. Enriquez, P. Brunet, P. Colinet, and J. H. Snoeijer, “Universality of tip singularity formation in freezing water drops,” *Phys. Rev. Lett.* **113**, 054301 (2014).
- <sup>14</sup>K. W. Kolasinski, “Solid structure formation during the liquid/solid phase transition,” *Curr. Opin. Solid State Mater. Sci.* **11**, 76–85 (2007).
- <sup>15</sup>S. Schiaffino and A. A. Sonin, “Motion and arrest of a molten contact line on a cold surface: An experimental study,” *Phys. Fluids* **9**, 2217–2226 (1997).
- <sup>16</sup>S. Schiaffino and A. A. Sonin, “Molten droplet deposition and solidification at low weber numbers,” *Phys. Fluids* **9**, 3172 (1997).
- <sup>17</sup>F. Tavakoli, S. H. Davis, and H. P. Kavehpour, “Freezing of supercooled water drops on cold solid substrates: initiation and mechanism,” *J. Coat. Technol. Res.* **12**, 869–875 (2015).

- <sup>18</sup>T. Vu, G. Tryggvason, S. Homma, and J. Wells, “Numerical investigations of drop solidification on a cold plate in the presence of volume change,” *Int. J. Multiph. Flow* **76**, 73–85 (2015).
- <sup>19</sup>H. Zhang, Y. Zhao, R. Lv, and C. Yang, “Freezing of sessile water droplet for various contact angles,” *Int. J. Therm. Sci.* **101**, 59–67 (2016).
- <sup>20</sup>Y. Hagiwara, S. Ishikawa, R. Kimura, and K. Toyohara, “Ice growth and interface oscillation of water droplets impinged on a cooling surface,” *J. Cryst. Growth* **468**, 46–53 (2017).
- <sup>21</sup>X. Zhang, X. Wu, J. Min, and X. Liu, “Modelling of sessile water droplet shape evolution during freezing with consideration of supercooling effect,” *Appl. Therm. Engin.* **125**, 644–651 (2017).
- <sup>22</sup>T. Vu, “Axisymmetric forced convection solidification of a liquid drop on a cold plate,” *Int. J. Multiph. Flow* **107**, 104–115 (2018).
- <sup>23</sup>Z. Jin, X. Cheng, and Z. Yang, “Experimental investigation of the successive freezing processes of water droplets on an ice surface,” *Int. J. Heat Mass Transf.* **107**, 906–915 (2017).
- <sup>24</sup>M. B. Short, J. C. Baygents, and R. E. Goldstein, “A free-boundary theory for the shape of the ideal dripping icicle,” *Phys. Fluids* **18**, 083101 (2006).
- <sup>25</sup>A. S.-H. Chen and S. W. Morris, “Experiments on the morphology of icicles,” *Phys. Rev. E* **83**, 026307 (2011).
- <sup>26</sup>A. S.-H. Chen and S. W. Morris, “On the origin and evolution of icicle ripples,” *New J. Phys.* **15**, 103012 (2013).
- <sup>27</sup>P. Claudin, H. Jarry, G. Vignoles, M. Plapp, and B. Andreotti, “Physical processes causing the formation of penitentes,” *Phys. Rev. E* **92**, 033015 (2015).
- <sup>28</sup>V. Lunardini, *Heat Transfer with Freezing and Thawing* (Elsevier, 1991).